Journal of Computational Acoustics,

SCATTERING NEAR A PLANE INTERFACE USING A GENERALIZED METHOD OF IMAGES APPROACH

ARNAUD COATANHAY
E ^{3}I ^{2}, ENSIETA, 2 rue François Verny, 29806 Brest Cedex 9, France
E-mail: coatanar@ensieta.fr

JEAN-MARC CONOIR
LAUE, UMR 6068, IUT, Pl Robert Schuman BP 4006, 76610 Le Havre, France
E-mail: Jeanmarc.Conoir@iut-lehavre.fr

Received (to be inserted
Revised by Publisher)

A new method for predicting the scattered acoustic field due to a plane wave incident upon an infinitely long cylinder lying near an penetrable plane interface is presented. The method generalizes the method of images which is restricted to rigid and soft plane interfaces. Validity domains, physical interpretations, simulations and numerical results are described for sedimentary medium-fluid plane interfaces. And, they are well compared with high frequency asymptotic results based on the Geometrical Theory of Diffraction(G.T.D.).

1. Introduction

As for sonar detection, medical imaging, geophysical exploration or nondestructive testing, the estimation of the scattering by an object in the vicinity of a plane interface constitutes one of the most common problem in acoustic. As the case may be, the object could be a mine close the sea-bed, an inhomogeneity embedded beneath a plane surface or any other physical problem. To estimate the acoustic field given by the scatterer-interface system, several standard approaches have been developed: finite elements, finite differences and boundary integral equation methods (BIEM) [1], for example. Nevertheless, these methods could be considered as a pure numerical point of view. A numerical estimation of the scattered field can be computed, but physical interpretations are not easy to make. Moreover, these methods often rise computational tractability problems. However, the ray model or modal theory can give an intuitive theoretical model for the complex scatterer-interface interaction, but the application involve many restrictions on use: high frequency and simple scatterer for the ray model approximation, or simple boundary condition at the plane interface for the modal theory. In this paper, we point out the interaction between the object and the plane interface, and we define a generalized approach based on modal theory, that requires fewer limitations and assumptions.

Actually, this study deals with the scattering of an acoustic plane wave by a cylindrical object lying near an elastic plane interface as shown in figure (1). In theory, no particular assumption is made about the cylindrical object that could be rigid, soft or elastic. More, the cross section is not limited to the circular case. In the following, the cylindrical object will be simply called "cylinder".

When the plane interface is of the rigid or soft type, this situation can be modeled with modal theory using the method of images. This method consists in replacing the scattering coming from the plane interface with the scattering coming from the image cylinder mirrored by the plane interface. The use of the method of images in acoustics is presented in [2,3,4,5]. The originality of our study results in the fact that the plane interface is not presupposed to be of the rigid or soft type.

In this case, it is no longer possible to use the standard method of images. So, we have to handle both the cylindrical and plane geometries in order to calculate the scattering process. On the one hand, we have to determine the reflection by the plane interface of the cylindrical waves coming from the cylinder. On the other hand, we have to determine the scattering by the cylinder of a plane wave spectrum coming from the interface. Afterward, it remains to merge these two types of interactions in order to describe the scattering by the cylinder-interface system. The scattering by the cylinder-interface system involves multiple interactions between the cylinder and the plane interface. Overall, the incident wave strikes the cylinder (or the plane interface) and then infinitely navigates between the cylinder and the plane interface. As the wave radiates toward the observer each time it strikes the cylinder or the interface, the global scattering by the cylinder-interface system can be obtained by adding all these multiple radiations.

With regard to the modal theory, the main difficulty stands in the study of the reflection of cylindrical waves by a neither rigid nor soft plane interface. To solve this problem, we decompose the considered cylindrical wave into its plane wave spectrum in order to calculate the reflection by the plane interface. The plane wave spectrum is obtained with the use of the Sommerfeld's integral expressions of Hankel's functions. Assuming the superposition principle, each reflected plane wave of the spectrum is determined with the reflection coefficient of the plane interface. Afterward, the so obtained reflected plane wave spectrum is written in the form of cylindrical waves in order to calculate its scattering by the cylinder. This last process is performed using the decomposition of the plane interface reflection coefficient in a Fourier's series. These different steps and the multiple radiation summation constitute the governing idea of our methodology.

After a detailed theoretical description of our approach, the influence of the waves scattered by the cylinder over the plane interface becomes more explicit. In a theoretical point of view, our theory can easily express the reflection of cylindrical waves coming from the cylinder center by the plane interface. In consequence, our study leads to an original expression of the Green's function for Helmholtz equation in the half-space. Moreover, this expression is used to evaluate our cylinder-plane interface model and assess its domain of validity. Then, numerical results are presented and compared to those obtained with the

ray model approach.

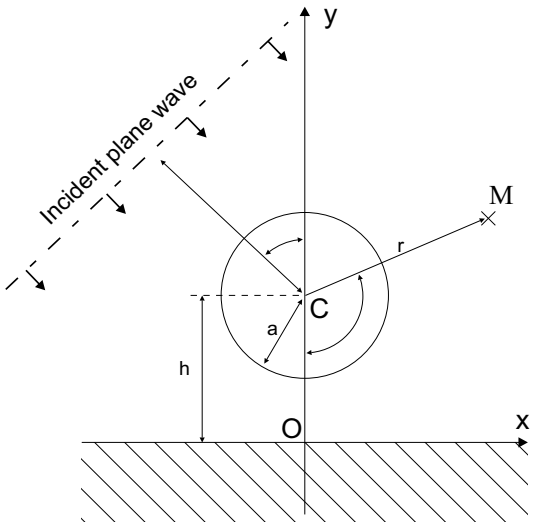

Fig. 1. Geometry of cylinder-interface system: α is the angle of incidence, C is the center of the cylinder, (r, θ) are the polar coordinates of the observer M, O is the origin of Cartesian coordinates and h is the distance of the cylinder center from the interface.

2. Description of the problem

Figure (1) illustrates the geometry of the problem: an infinite cylinder is lying parallel above a plane interface, and the incident wave direction is in the perpendicular plane. These assumptions reduce the physical problem to a two-dimensional one.

The origin C of the cylindrical coordinate system (r, θ) coincides with the cylinder center. The distance from C to the plane interface is denoted by h . The image of the cylinder center mirrored by the plane interface lies below the plane interface. This image point denoted by C_s is the center of a second cylindrical coordinate system (r_s, θ_s). The index s stands for symmetric (with regard to the plane interface). The wave number in the fluid medium is defined as $k = \omega/c_1$ where ω is the angular frequency and c_1 the sound speed. The scattered acoustic field is calculated at the observation point, denoted by M, above the plane interface.

In the following, we consider an incident plane wave which impinges the cylinder-interface system with the incident angle α (see figure 1). The time dependent factor $e^{-i\omega t}$ being suppressed, the considered incident wave can be expressed, in Cartesian and polar coordinates, as follows [6]:

$$\mathbf{p}_{inc} = e^{ik(x\sin\alpha - (y-h)\cos\alpha)} = \sum_{n=-\infty}^{+\infty} i^n e^{-in\alpha} J_n(kr)\, e^{in\theta} \tag{2.1}$$

where J_n are the Bessel functions of first kind, and i such $i^2 = -1$.

The plane interface is acoustically characterized by the reflection coefficient of plane waves [7,8,9,10]. Let $R(\alpha)$ be the reflection coefficient depending on angle α. Thus, the reflected plane wave may be written as:

$$\begin{array}{rcl} \mathbf{p}_R & = & R(\alpha)\, e^{ik(x\sin\alpha+(y+h)\cos\alpha)} = R(\alpha)\, e^{ik(x\sin\alpha+(y-h)\cos\alpha)} \cdot e^{ik\ 2h\cos\alpha} \\ & = & R(\alpha)\, e^{ik(x\sin(\pi-\alpha)-(y-h)\cos(\pi-\alpha))} \cdot e^{ik\ 2h\cos\alpha} \end{array} \tag{2.2}$$

In a theoretical point of view, the knowledge of the explicit expression of $R(\alpha)$ is not relevant for the mathematical analysis developed in the paper. $R(\alpha)$ is only assumed to be a known function. In fact, the so defined plane interface can be either a single interface or a multilayered one. Consequently, the reflection coefficient can also depend on the frequency, the thickness and the material properties of the different layers.

Taking into account direct and reflected incident wave, the cylinder is struck by two plane waves. The sum of these two waves, called global incident wave and denoted $\mathbf{p}_{ginc}$, may be expressed in the form of a modal series [6]:

$$\mathbf{p}_{ginc} = \mathbf{p}_{inc} + \mathbf{p}_R = \sum_{n=-\infty}^{+\infty} i^n \left[e^{-in\alpha} + R(\alpha)\, e^{ikd\cos\alpha} e^{-in(\pi-\alpha)} \right] J_n(kr)\, e^{in\theta} \tag{2.3}$$

where $d = 2h$ is the distance between C_s and C.

Let $\xi_n^{(\alpha)}$ and $\Psi_n^{(j)}$ be the components of the vectors $\vec{\xi}^{(\alpha)}$ and $\vec{\Psi}^{(j)}$ defined as follows:

$$\xi_n^{(\alpha)} = i^n \left[e^{-in\alpha} + R(\alpha)\, e^{ikd\cos\alpha} e^{-in(\pi-\alpha)} \right] \tag{2.4}$$

$$\Psi_n^{(j)} = J_n(kr)\, e^{in\theta} \tag{2.5}$$

where the superscript $^{(j)}$ stands for the J_n Bessel functions. Accordingly, the equation (2.3) can be rewritten as :

$$\mathbf{p}_{ginc} = \mathbf{p}_{inc} + \mathbf{p}_R = \left\langle \vec{\xi}^{(\alpha)}, \vec{\Psi}^{(j)} \right\rangle \tag{2.6}$$

where $\langle\ ,\ \rangle$ denotes the usual scalar product defined as (with a_n and b_n the components of vectors $\vec{a}$ and $\vec{b}$):

$$\left\langle \vec{a}, \vec{b} \right\rangle = \sum_{n=-\infty}^{+\infty} a_n b_n \tag{2.7}$$

Afterward, for the sake of simplicity, modal series will be commonly expressed in algebraic form with the use of the scalar product defined in Eq. (2.7).

By knowing the mathematical expression of an incident wave, the direct acoustic field scattered by a cylinder can be determined using modal theory. For a circular cross section cylinder, the acoustic properties are given by the modal scattering amplitudes denoted by T_n (the index n denotes the mode of vibration). Letting $\mathbf{p}_i$ an incident wave:

$$\mathbf{p}_i = \sum_{n=-\infty}^{+\infty} \xi_n \Psi_n^{(j)} = \left\langle \vec{\xi}, \vec{\Psi}^{(j)} \right\rangle \tag{2.8}$$

the scattering by the circular cross section cylinder takes the form of this following expression [11,12,13,14]:

$$\mathbf{p}_s = \sum_{n=-\infty}^{+\infty} \xi_n T_n \Psi_n^{(1)} \tag{2.9}$$

$$\mathbf{p}_s = \left\langle \vec{\xi}, \mathbf{T} \cdot \vec{\Psi}^{(1)} \right\rangle \tag{2.10}$$

where the modal scattering amplitudes T_n $(-\infty < n < +\infty)$ are the components of the diagonal $\mathbf{T}$ operator. In practice, the scattering amplitudes T_n are obtained with the use of the classical separation of variables. The components $\Psi_n^{(1)}$ of the vector $\vec{\Psi}^{(1)}$ are the outgoing cylindrical waves defined as:

$$\Psi_n^{(1)} = H_n^{(1)}(kr)\, e^{in\theta} \tag{2.11}$$

where $H_n^{(1)}$ are the Hankel functions of the first kind (denoted by the superscript $^{(1)}$). These outgoing cylindrical waves satisfy the Sommerfeld far field boundary conditions [6].

For non circular cross section cylinder, the linear $\mathbf{T}$ operator is no longer a diagonal operator, but the expression of the field scattered by the cylinder in Eq. (2.10) is still appropriate. In the field of the Resonance Scattering Theory (R.S.T.), the operator is sometimes called the transition matrix.

To sum up this first part, the geometrical configuration is characterized by only one parameter: the h distance of the cylinder center from the interface. And, the scattering by a cylinder or by a plane interface can be modeled with the knowledge of the $R(\alpha)$ reflection coefficient of the plane interface and the $\mathbf{T}$ transition matrix of the cylinder. We have just to note that the way to obtain $R(\alpha)$ and $\mathbf{T}$ is usually well known and a large amount of papers are devoted to their calculation [10,15,16].

3. Mathematical model

3.1. *Reflection of cylindrical waves*

As previously seen, the scattering by a cylinder can be expressed in the form of a modal series (Eq. (2.9)), which is nothing but a linear superposition of the outgoing cylindrical waves defined in Eq. (2.11) [11,12,13,14]. Accordingly, the study of the reflection by the plane interface of waves coming from the cylinder can be deduced from the analysis of an outgoing cylindrical waves reflection. So, let us consider an outgoing cylindrical wave $\Psi_n^{(1)}$ where n is a given mode of vibration.

The Hankel function of the first kind of order n can be written as [6,17]

$$H_n^{(1)}(kr) = \frac{1}{\pi} \int_{W_0} e^{ikr\cos\omega} e^{in(\omega-\pi/2)}\, d\omega \tag{3.12}$$

where the W_0 contour starts from $W_0^s + i\infty$ with $-\pi < W_0^s < 0$ and ends at $W_0^f - i\infty$ with $0 < W_0^f < +\pi$ (the super script s and f stand for start and final). According to

Sommerfeld [17], by introducing the new variable θ_k as follows

$$\omega = \theta_k - \theta \tag{3.13}$$

the above integral can be written as

$$\Psi_n^{(1)} = H_n^{(1)}(kr)\, e^{in\theta} = \frac{1}{\pi} \int_W e^{ik(x\sin\theta_k - (y-h)\cos\theta_k)} e^{in(\theta_k - \pi/2)}\, d\theta_k \tag{3.14}$$

where W is the Sommerfeld contour starting from $-\pi/2 + i\infty$ and ending at $\pi/2 - i\infty$ (see figure 2).

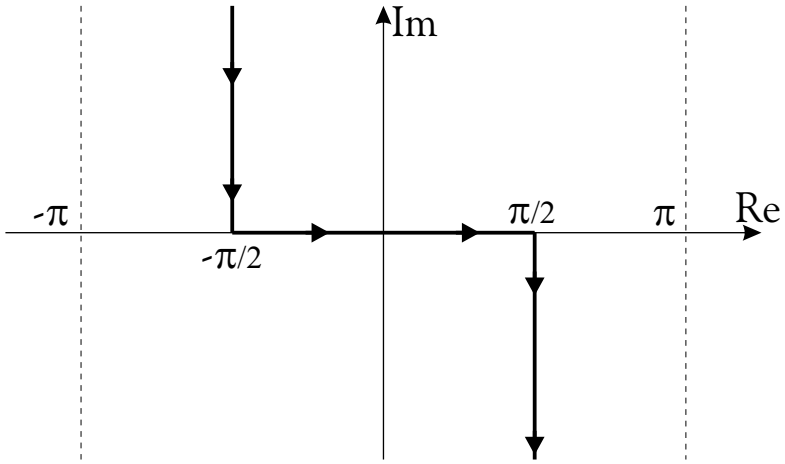

Fig. 2. Sommerfeld path of integration.

In a physical point of view, θ_k represents the incident angle of a plane wave (θ_k is similar to α defined in Eq. (2.1)). Hence, any considered outgoing cylindrical wave can be represented as a plane wave spectrum. This result enables us to determine the reflection of Ψ_n^1 by a plane interface using the principle of superposition [10]. From this principle, the reflection of the considered cylindrical wave $\Psi_n^{(1)}$ takes the following form (see Eq. (2.2)):

$$\Psi_{R,n}^{(1)} = \frac{1}{\pi} \int_W R(\theta_k)\, e^{ik(x\sin\theta_k + (y+h)\cos\theta_k)} e^{in(\theta_k - \pi/2)}\, d\theta_k \tag{3.15}$$

This equation give an analytical expression for a reflected cylindrical wave. Nevertheless, this mathematical expression does not constitute an appropriate model to investigate multiple interactions between the cylinder and plane interface. As a matter of fact, to study the scattering by the cylinder, we are going to express $\Psi_{R,n}^{(1)}$ as a linear superposition of

outgoing cylindrical waves $\Psi_n^{(s)}$ coming from the C_s image point. Using the previously seen Sommerfeld's integral, these $\Psi_n^{(s)}$ outgoing cylindrical waves can be easily written as:

$$\Psi_n^{(s)} = H_n^1(kr_s)\, e^{in\theta_s} = \frac{1}{\pi} \int\limits_W e^{ik(x\sin\theta_k + (y+h)\cos\theta_k)} e^{in(\theta_k - \pi/2)}\, d\theta_k \tag{3.16}$$

More, the $\Psi_n^{(s)}$ elements are the components of the vector $\vec{\Psi}^s$.

To express $\Psi_{R,n}^{(1)}$ as a linear superposition of $\Psi_n^{(s)}$ components, we suppose that $R(\theta_k)$ can be expanded in a Fourier series in θ_k as follows:

$$R(\theta_k) = \sum_{m=-\infty}^{+\infty} R_m e^{im\theta_k} \tag{3.17}$$

In fact, this assumption rises fundamental problems that will be examined later in the discussion section . Yet, on this assumption, inserting Eq. (3.17) into Eq. (3.15) leads to:

$$\Psi_{R,n}^{(1)} = \sum_{m=-\infty}^{+\infty} R_m i^m \left[\frac{1}{\pi} \int\limits_W e^{ik(x\sin\theta_k + (y+h)\cos\theta_k)} e^{i(n+m)(\theta_k - \pi/2)}\, d\theta_k \right] \tag{3.18}$$

with the transposition between integration and summation. Let R_{mn} be the components of the reflection $\mathbf{R}$ operator defined as:

$$R_{mn} = i^{m-n} R_{m-n} \tag{3.19}$$

More intuitively, the reflection $\mathbf{R}$ operator looks like:

$$\mathbf{R} = \begin{pmatrix} R_0 & -iR_{-1} & -R_{-2} & iR_{-3} & \ddots \\ iR_1 & R_0 & -iR_{-1} & -R_{-2} & iR_{-3} \\ -R_2 & iR_1 & R_0 & -iR_{-1} & -R_{-2} \\ -iR_3 & -R_2 & iR_1 & R_0 & -iR_{-1} \\ \ddots & -iR_3 & -R_2 & iR_1 & R_0 \end{pmatrix} \tag{3.20}$$

Thus, the reflected cylindrical waves may be written as:

$$\Psi_{R,n}^{(1)} = \sum_{m=-\infty}^{+\infty} R_{m-n} i^{m-n} \Psi_m^{(s)} \tag{3.21}$$

Letting $\Psi_{R,n}^{(1)}$ the components of the vector $\vec{\Psi}_R^{(1)}$, Eq. (3.21) give the algebraic relation:

$$\vec{\Psi}_R^{(1)} = \mathbf{R} \cdot \vec{\Psi}^{(s)} \tag{3.22}$$

If rigid or soft interfaces are considered, $R(\theta_k) = 1$ or $R(\theta_k) = -1$ respectively. So, in these cases, Eq. (3.22) is reduced to:

$$\vec{\Psi}_R^{(1)} = \pm \vec{\Psi}^{(s)} \tag{3.23}$$

Eventually, we defined the **R** linear operator that enables to express the reflection of a cylindrical waves coming from the cylinder (considered as series of $\Psi_n^{(1)}$ terms) in the form of a series of $\Psi_m^{(s)}$ terms.

3.2. *Double interaction*

Previously, we described the reflection of $\Psi_n^{(1)}$ by the plane interface and we gave the expression for $\Psi_{R,n}^{(1)}$. Now, we consider the scattering of $\Psi_{R,n}^{(1)}$ by the cylinder. This scattered acoustic field designated by $\Psi_{RS,n}^{(1)}$ is what we call the double interaction: an interaction with the interface (reflection) and with the cylinder (scattering). This paragraph is devoted to the determination of this double interaction.

Due to the linearity, this problem consists in calculating the scattering of a $\Psi_n^{(s)}$ component by the cylinder. To this end, $\Psi_n^{(s)}$ has to be written as a linear superposition of cylindrical waves $\Psi_n^{(j)}$. This problem is solved with the use of the Graf theorem (see[18] page 363), also called addition theorem, from which the following relation is obtained:

$$\Psi_n^{(s)} = \sum_{m=-\infty}^{+\infty} H_{m+n}^1(kd)\,\Psi_m^{(j)} \tag{3.24}$$

We can define the Graf linear operator denoted by **G** whose components G_{nm} are defined as follow:

$$G_{nm} = H_{m+n}^{(1)}(kd) \tag{3.25}$$

More intuitively, the Graf linear operator **G** looks like:

$$\mathbf{G} = \begin{pmatrix} \ddots & H_{-3}^{(1)}(kd) & H_{-2}^{(1)}(kd) & H_{-1}^{(1)}(kd) & H_0^{(1)}(kd) \\ H_{-3}^{(1)}(kd) & H_{-2}^{(1)}(kd) & H_{-1}^{(1)}(kd) & H_0^{(1)}(kd) & H_1^{(1)}(kd) \\ H_{-2}^{(1)}(kd) & H_{-1}^{(1)}(kd) & H_0^{(1)}(kd) & H_1^{(1)}(kd) & H_2^{(1)}(kd) \\ H_{-1}^{(1)}(kd) & H_0^{(1)}(kd) & H_1^{(1)}(kd) & H_2^{(1)}(kd) & H_3^{(1)}(kd) \\ H_0^{(1)}(kd) & H_1^{(1)}(kd) & H_2^{(1)}(kd) & H_3^{(1)}(kd) & \ddots \end{pmatrix} \tag{3.26}$$

Thus, letting $\vec{\Psi}^{(s)}$ whose components are $\Psi_n^{(s)}$, the Eq. (3.24) takes the algebraic form:

$$\vec{\Psi}^{(s)} = \mathbf{G} \cdot \vec{\Psi}^{(j)} \tag{3.27}$$

Finally, straight from Eqs. (2.8,2.10,3.22,3.27), it follows that the double interaction vector $\vec{\Psi}_{RS}^{(1)}$ of components $\Psi_{RS,n}^{(1)}$ is given by:

$$\vec{\Psi}_{RS}^{(s)} = \mathbf{R} \cdot \mathbf{G} \cdot \mathbf{T} \cdot \vec{\Psi}^{(1)} = \mathbf{D} \cdot \vec{\Psi}^{(1)} \tag{3.28}$$

where the **D** operator defined in Eq. (3.28) is called operator of double interaction.

3.3. *Scattering by the cylinder-interface system*

The scattering by the cylinder-interface system involves two contributions: one coming from the cylinder and the other from the interface. The cylinder contribution is due to the incident wave $\mathbf{p}_{ginc}$ defined in Eq. (2.6) which strikes the cylinder and then infinitely navigates between the cylinder and the plane interface. Consequently, the contribution of order 0 resulting from the direct scattering by the cylinder of the incident wave $\mathbf{p}_{ginc}$ is expressed as:

$$\mathbf{p}_{cyl}^{(0)} = \left\langle \vec{\xi}^{(\alpha)}, \mathbf{T} \cdot \vec{\Psi}^{(1)} \right\rangle \tag{3.29}$$

The contribution of order 1 is due to the reflection by the interface and the scattering by the cylinder (double interaction) of the contribution of order 0, and so on. As a result, straight from Eq. (3.28), the contribution of order n is given by:

$$\mathbf{p}_{cyl}^{(n)} = \left\langle \vec{\xi}^{(\alpha)}, \mathbf{T} \cdot \mathbf{D}^n \cdot \vec{\Psi}^{(1)} \right\rangle \tag{3.30}$$

The full contribution of the cylinder is nothing but the sum of each contribution of order n=0,1,2,...:

$$\mathbf{p}_{cyl} = \sum_{n=0}^{+\infty} \left\langle \vec{\xi}^{(\alpha)}, \mathbf{T} \cdot \mathbf{D}^n \cdot \vec{\Psi}^{(1)} \right\rangle \tag{3.31}$$

where $_{cyl}$ stands for cylinder.

Using the linearity of the scalar product, Eq. (3.31) can be written as

$$\mathbf{p}_{cyl} = \left\langle \vec{\xi}^{(\alpha)}, \mathbf{T} \cdot (\mathbf{I} - \mathbf{D})^{-1} \cdot \vec{\Psi}^{(1)} \right\rangle \tag{3.32}$$

where $\mathbf{I}$ is the unity matrix.

Without considering the reflected plane wave $\mathbf{p}_R$ defined in Eq. (2.2), the full contribution coming from the plane interface is due to the reflection of cylindrical waves coming from the cylinder. Hence, using Eq. (3.22) and the linearity of the scalar product, Eq. (3.32) leads to the following expression (int stands for interface):

$$\mathbf{p}_{int} = \left\langle \vec{\xi}^{(\alpha)}, \mathbf{T} \cdot (\mathbf{I} - \mathbf{D})^{-1} \cdot \mathbf{R} \cdot \vec{\Psi}^{(s)} \right\rangle \tag{3.33}$$

Finally, the scattering of an incident plane wave by the cylinder-interface system is given by:

$$\mathbf{p}_{sys} = \mathbf{p}_R + \mathbf{p}_{cyl} + \mathbf{p}_{int} = \mathbf{p}_R + \left\langle \vec{\xi}^{(\alpha)}, \mathbf{T} \cdot (\mathbf{I} - \mathbf{D})^{-1} \cdot \left(\vec{\Psi}^{(1)} + \mathbf{R} \cdot \vec{\Psi}^{(s)} \right) \right\rangle \tag{3.34}$$

This expression takes into account every mutual interactions between the cylinder and the interface.

3.4. *Comparison with the method of images*

In the case of rigid and soft plane interfaces (r and s stand for rigid and soft), the reflection $\mathbf{R}$ operator is reduced to $\mathbf{R}^{(r,s)} = \pm\mathbf{I}$ (see Eq. (3.23)) and the double interaction $\mathbf{D}$ operator

to $\mathbf{D}^{(r,s)} = \pm\mathbf{G}\cdot\mathbf{T}$(see Eq. (3.28)), respectively. In the same way, the reflected wave $\mathbf{p}_R$ which is designated here by $\mathbf{p}_R^{(r,s)}$ takes the following form

$$\mathbf{p}_R^{(r,s)} = \pm e^{ik(x\sin\alpha+(y+h)\cos\alpha)} \tag{3.35}$$

where $\mathbf{p}_R^{(r,s)}$ is the "image" of the incident plane wave.

So, the global scattering by the cylinder near a rigid or soft interface can be reduced to the simple form:

$$\mathbf{p}_{sys} = \mathbf{p}_R^{(r,s)} + \left\langle \vec{\xi}^{(\alpha)}, \mathbf{T}\cdot\left(\mathbf{I}-\mathbf{D}^{(r,s)}\right)^{-1}\cdot\vec{\Psi}^{(1)}\right\rangle \pm \left\langle \vec{\xi}^{(\alpha)}, \mathbf{T}\cdot\left(\mathbf{I}-\mathbf{D}^{(r,s)}\right)^{-1}\cdot\vec{\Psi}^{(s)}\right\rangle \tag{3.36}$$

which is the solution obtained using the method of images [4]. Indeed, $\vec{\Psi}^{(s)}$ and $\vec{\Psi}^{(1)}$ represent the outgoing cylindrical waves coming from the cylinder center C or its image C_s. The "rigid or soft solution" (3.36) is the sum of two contributions due to a cylinder and its image mirrored by the interface (or the opposite one).

In consequence, our theoretical approach constitutes a generalization of the method of the images, called (G.M.I.).

3.5. *The two-dimensional Green function*

In this section, the cylinder is replaced by a 2D point source located at C (see figure (1)), i.e. a line parallel above the interface emitting an unitary outgoing cylindrical wave. The acoustic field generated in the half-plane containing the source is the solution of the following equation:

$$\bigtriangledown^2 G + k^2 G = -\delta\left(\vec{r}\right) \tag{3.37}$$

where G verifies both the boundary conditions at the plane interface and the Sommerfeld boundary condition to infinity:

$$\lim_{r\to+\infty}\sqrt{r}\left[\frac{\partial G}{\partial r} - ikG\right] = 0 \tag{3.38}$$

In Eq. (3.37), δ is the two-dimensional Dirac function and $\vec{r}$ is the position vector related to the C point source .

Mathematically, the G solution is known as the 2D Green function in the half-plane. A common way to determine this Green function is to assume that:

$$G = \frac{1}{4i}\left[\Psi_0^{(1)} + \widetilde{G}\right] \tag{3.39}$$

where $\Psi_0^{(1)}/4i$ (which is the well known two-dimensional Green function in the infinite space) verifies both Eq. (3.37) and the Sommerfeld boundary condition, and $\widetilde{G}$ verifies both the homogeneous Helmholtz equation and the Sommerfeld boundary condition. Obviously, the particular $\widetilde{G}$ solution is chosen so that G verifies the boundary conditions on the plane

interface. Physically, $\widetilde{G}$ is nothing else but the reflection of the incident wave $\Psi_0^{(1)}$. Using previous notations, $\widetilde{G} = \Psi_{R,0}^{(1)}$ and the Green function can be written either as a plane wave spectrum (see Eq. (3.15)):

$$G = \frac{1}{4i\pi} \int_W \left[e^{ik(x\sin\theta_k - (y-h)\cos\theta_k)} + R(\theta_k)\, e^{ik(x\sin\theta_k + (y+h)\cos\theta_k)} \right] d\theta_k \tag{3.40}$$

or as a modal series involving outgoing cylindrical waves (see Eq. (3.21) with $n = 0$)

$$G = \frac{1}{4i\pi} \left[\Psi_0^{(1)} + \sum_{m=-\infty}^{+\infty} R_m i^m \Psi_m^{(s)} \right] \tag{3.41}$$

Eq. (3.40) is very similar to that of reference [19], except that integration is performed over angles rather than wave numbers. The representation of the Green function given in Eq. (3.40) is rather usual while, as far we are aware, the Eq. (3.41) is an original expression.

4. Discussion and numerical results

According to the algebraic theory previously described (G.M.I.), the scattering problem raised by a cylindrical object lying near a plane interface can be reduced to the determination of three linear operators: **T**,**G** and **R**. The **T** operator provides a synthetic expression of the scattering properties with regard to the cylinder, and the **G** characterizes the geometrical configuration of the interface-cylinder system (the distance between the cylinder and the interface). The **T** and **G** operators are commonly used in modal theory, and do not require particular mathematical precautions to take.

On the contrary, the generalized method of images (G.M.I.) introduces the **R** linear operator that describes the scattering properties of the interface, and this linear operator is based on a mathematical assumption. Here, we are going to analyze the theoretical limits of this assumption. Then, we point out the numerical consequences about the G.M.I. approach and specify the validity of the associated theory.

4.1. *Theoretical limitations*

To introduce the **R** operator, we assume that the reflection coefficient $R(\theta)$ could be expanded in a Fourier series in θ_k as follows:

$$R(\theta_k) = \sum_{m=-\infty}^{+\infty} R_m e^{im\theta_k} \ . \tag{4.42}$$

For a real variable, the equation (4.42) raise no particular problem. But in complex space, this statement becomes open to criticism. Letting $z = e^{i\theta_k}$, the Fourier series leads to a Laurent series:

$$R(\theta_k) = \sum_{m=-\infty}^{+\infty} R_m z^m \ . \tag{4.43}$$

The convergence of the Laurent series is proved in an annular domain: the modulus of z has to be greater than a maximum and lower than a minimum. So, for θ_k variable, the equation (4.42) is only valid on a band domain around the real axis. The width of this band depends on the decrease of the R_m coefficients. When this R_m series decrease very fast, the convergence domains become wider, and vice versa. In fact, the R_m coefficients decrease fast when the $R(\theta_k)$ function is smooth.

The G.M.I. theory is based on a decomposition of cylindrical waves into plane wave spectra, and the use of the Sommerfeld integral. The problem is that the Sommerfeld integral path (see figure 2) can not be restricted to a finite domain. Hence, in a schematic way, the interface modeling can be split into three possibilities: In the first case, the reflection coefficient function is very smooth (rigid or soft interface for example). Then, the width of the convergence domains could be infinite and the G.M.I. theory is absolutely exact. In the second case, the reflection coefficient is smooth enough, then the convergence band is wide and the G.M.I. constitutes an excellent approximation of the reality. In the last case, the reflection coefficient is an irregular function. The convergence band is narrow and the G.M.I. must not be used.

In practice, the situation is often less clear-cut. And, to confront the G.M.I. approach with actual physical situations, we are going to analyze three interfaces with numerical estimations: two fluid-fluid interfaces and a fluid-solid interface.

4.2. *Numerical study of different interfaces*

An efficient way to estimate the validity of G.M.I. approach for different type interfaces, is to determine the pressure field caused by a source point close a plane interface. The previous section showed that the two-dimensional Green function in the half-plane could be expressed as an integral expression:

$$G = \frac{1}{4i\pi} \int\limits_W \left[e^{ik(x\sin\theta_k - (y-h)\cos\theta_k)} + R(\theta_k)\, e^{ik(x\sin\theta_k + (y+h)\cos\theta_k)} \right] d\theta_k \tag{4.44}$$

or, with the use of G.M.I. theory, as a Fourier series:

$$G = \frac{1}{4i\pi} \left[\Psi_0^{(1)} + \sum_{m=-\infty}^{+\infty} R_m i^m \Psi_m^{(s)} \right] \tag{4.45}$$

Hence, the equality between the $R(\theta_k)$ function and its Fourier series can be assumed if the expression:

$$\widetilde{G}_1 = \int\limits_W R(\theta_k)\, e^{ik(x\sin\theta_k + (y+h)\cos\theta_k)}\, d\theta_k \tag{4.46}$$

is equivalent to:

$$\widetilde{G}_2 = \sum_{m=-\infty}^{+\infty} R_m i^m \Psi_m^{(s)} \tag{4.47}$$

If these two expressions were not equivalent, the difference between $\widetilde{G}_1$ and $\widetilde{G}_2$ could give an estimation of the approximation made in the G.M.I. theory. To numerically evaluate both expressions, we consider an observation point (M) moving above the interface at given altitude (between the interface and the point source), (see figure 3). The geometrical conditions are chosen so that the dimensionless product kr_s is equal to 10 when the M point is at the nearest position from the mirrored point source ($x_M = 0$). Then, the M point is shifted parallel to the interface so that the product kr_s reached about 100. Then, at each position of the observer, a numerical comparison between $\widetilde{G}_1$ and $\widetilde{G}_2$ can be easily made.

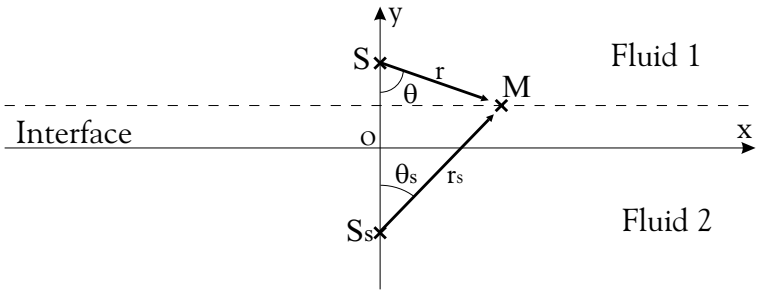

Fig. 3. Position of the observer in the vicinity of the interface: S is the point source, S_s is the point source mirrored by the interface, (r, θ) are polar coordinates related to the S point and (r_s, θ_s) are polar coordinates related to the S_s point.

4.2.1. *Fluid-fluid interface (1st case)*

For the first case, we suppose the source is embedded in sedimentary media approximated to a fluid media. The velocity c_1 and the density ρ_1 are respectively 1780 $m \cdot s^{-1}$ and 1320 $kg{\cdot}m^{-3}$. The second media is made up of standard water with velocity $c_2 = 1470\, m{\cdot}s^{-1}$ and density $\rho_2 = 1000\ kg \cdot m^{-3}$. Without lost of generality, the reflection coefficient for a fluid-fluid interface can be expressed in the analytic form [10]:

$$R(\theta) = \frac{\rho_2/\rho_1 \cos\theta - \left[(c_1/c_2)^2 - \sin^2\theta\right]^{1/2}}{\rho_2/\rho_1 \cos\theta + \left[(c_1/c_2)^2 - \sin^2\theta\right]^{1/2}} \tag{4.48}$$

where the complex square root $[\cdot\cdot]^{1/2}$ is defined from the real one $\sqrt{\cdot\cdot}$ as follows:

$$\left[(c_1/c_2)^2 - \sin^2\theta\right]^{1/2} = \sqrt{(c_1/c_2)^2 - \sin^2\theta} \tag{4.49}$$

when $\sin\theta \leq c_1/c_2$, and

$$\left[(c_1/c_2)^2 - \sin^2\theta\right]^{1/2} = i\sqrt{\sin^2\theta - (c_1/c_2)^2} \tag{4.50}$$

when $\sin\theta \geq c_1/c_2$, in order to respect the vanishing of the transmitted wave as usually required [10].

It is noteworthy that, in the present numerical situation, the critical angle θ^c, defined as $\sin\theta^c = c_1/c_2$, does not exist in the real domain. The reflection coefficient $R(\theta)$ can be considered as a smooth function, and the amplitude of Fourier coefficients R_n related to this function quickly decrease to zero, (see figure 4). This rapid decrease involve a large convergence domains and leads to good conditions for G.M.I. use. However, the convergence domain is not unlimited, and we are faced with the divergence problem of the $\widetilde{G}_2$ modal series (4.47). As a matter of fact, the $\widetilde{G}_2$ expression looks like an asymptotic series. The series terms $R_m i^m \Psi_m^{(s)}$ are bounded as far as $m \leq kr_s$ but increase exponentially as soon as m is greater than kr_s.

Nevertheless, many previous studies showed that an asymptotic series often provide an accurate numerical approximation if it is truncated before the divergence point (kr_s for the present case) [20,21]. In a pragmatic way, we arbitrarily decided to take into account $R_m i^m \Psi_m^{(s)}$ terms if $-kr_s/2 \leq m \leq kr_s/2$.

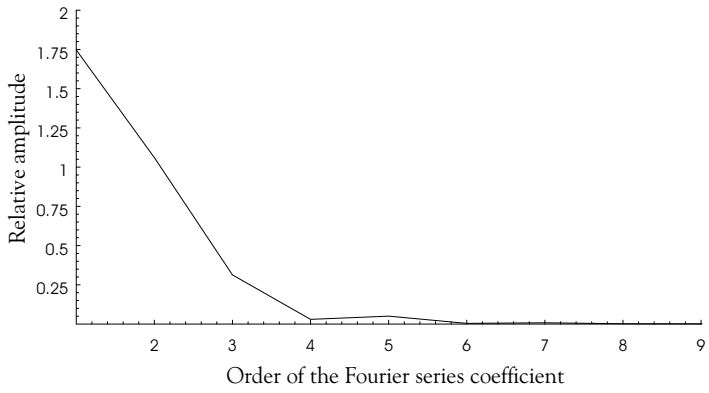

Fig. 4. Amplitude of Fourier coefficients in the first fluid-fluid interface case.

Figure (5) shows that the so obtained approximation of the $\widetilde{G}_2$ expression (dotted line) and the computed $\widetilde{G}_1$ integral expression (plain line) are very close. We can notice that the difference is negligible for high kr_s values and the maximum amplitude of the relative error is about 1 percent. For this numerical example, the G.M.I. approach must be consider as a very appropriate model.

4.2.2. *Fluid-fluid interface (2nd case)*

For the second numerical example, the situation uses the same media and same geometrical configuration, but the source is now embedded in the water beneath the sedimentary medium. In this part, the $_1$ index stands for the water and the $_2$ index for the sediment. The main difference from the first numerical example is that the critical angle exists in the

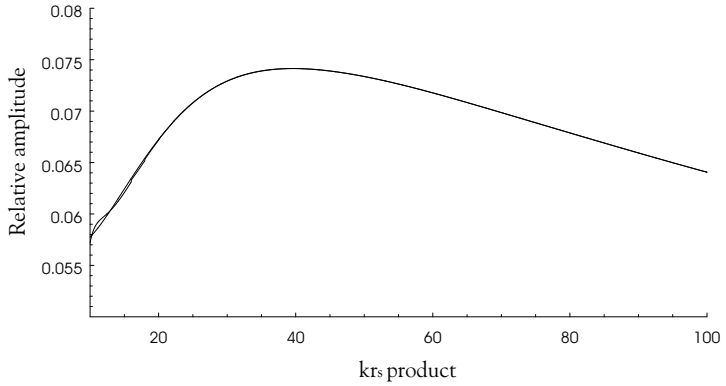

Fig. 5. Comparison between series (dotted line) and integral (plain line) expression of the Green function for the first fluid-fluid case.

real domain: $\theta^c = \arcsin(c_1/c_2)$.

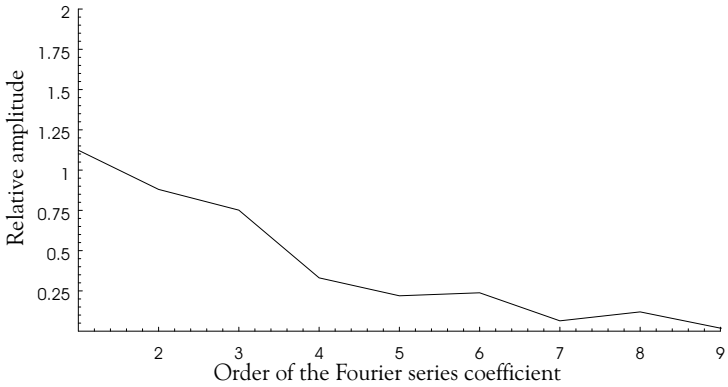

Fig. 6. Amplitude of Fourier coefficients in the second fluid-fluid interface case.

In a way, this critical angle can be considered as a loss of smoothness for the reflection coefficient $R(\theta)$ function. In consequence of this irregularity, the amplitude of the Fourier series decreases slower than the first case, (see figure 6). Thus, the convergence domain must be smaller and G.M.I. approach will provide less accurate numerical results. As a matter of fact, figure (7) shows that the error is still negligible for high kr_s values, but the numerical estimation is not correct for lower values. In the worst case, the amplitude of the relative error reach 40 percent.

However, it is worth noting that the smoothness of $R(\theta)$ function is greater if absorption phenomenon is taken into account (real case). In order to check this statement, we considered absorption for this fluid-fluid plane interface. This absorption is modeled by

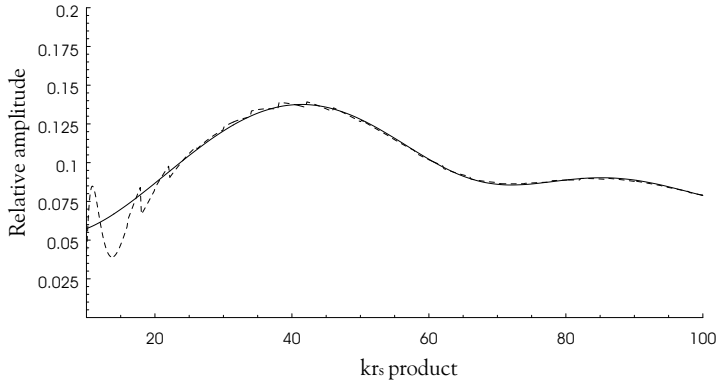

Fig. 7. Comparison between series (dotted line) and integral (plain line) expression of the Green function for the second fluid-fluid case.

considering the sound velocity as a complex value for the lower fluid [22]:

$$c_2^{(abs)} = c_2\,(1 - i\beta) \tag{4.51}$$

where β is the normalized absorption factor. The corresponding reflection coefficient is obtained from Eq. (4.48) by performing the analytic continuation of the complex square root so that it tends toward Eqs. (4.49,4.50) with the vanishing of β. In this way, using previous parameters, an absorption coefficient of $\beta = 0.1$ reduce the maximum amplitude of the worst case error from 40 to 18 percent.

About this second fluid-fluid interface example, we can conclude that, despite a lower accuracy, G.M.I. is still an appropriate numerical model especially for higher frequencies.

4.2.3. *Fluid-solid interface*

For fluid-fluid interfaces, G.M.I. seems to be an appropriate numerical method. On the other hand, fluid-solid interface involve a far more complex expression (4.52) for the reflection coefficient function $R\,(\theta)$:

$$R\,(\theta) = \frac{\frac{\rho_2}{\rho_1}\cos\theta\left(\left(\left(\frac{c_1}{c_{L2}}\right)^2 - 2\sin^2\theta\right)^2 + 4\sin^2\theta\sqrt{\left(\frac{c_1}{c_{L2}}\right)^2 - \sin^2\theta}\sqrt{\left(\frac{c_1}{c_{T2}}\right)^2 - \sin^2\theta}\right)\cdots}{\frac{\rho_2}{\rho_1}\cos\theta\left(\left(\left(\frac{c_1}{c_{L2}}\right)^2 - 2\sin^2\theta\right)^2 + 4\sin^2\theta\sqrt{\left(\frac{c_1}{c_{L2}}\right)^2 - \sin^2\theta}\sqrt{\left(\frac{c_1}{c_{T2}}\right)^2 - \sin^2\theta}\right)\cdots} \\ \frac{\cdots - \left(\frac{c_1}{c_{T2}}\right)^4\sqrt{\left(\frac{c_1}{c_{L2}}\right)^2 - \sin^2\theta}}{\cdots + \left(\frac{c_1}{c_{T2}}\right)^4\sqrt{\left(\frac{c_1}{c_{L2}}\right)^2 - \sin^2\theta}} \tag{4.52}$$

where ρ_1, ρ_2, c_1, c_{L2} and c_{T2} are respectively the density of fluid and solid media, the velocity of fluid media, the longitudinal and transversal velocity of solid media. In this case,

the smoothness of the $R(\theta)$ function is far worse than the previous fluid-fluid cases. As a numerical example, the fluid media is water ($\rho_1 = 1000\ kg \cdot m^{-3}$, $c_1 = 1470\ m \cdot s^{-1}$) and the solid media is aluminum ($\rho_2 = 2790\ kg \cdot m^{-3}$, $c_{L2} = 6557\ m \cdot s^{-1}$, $c_{T2} = 3128\ m \cdot s^{-1}$). Figure (8) shows that the amplitude of the Fourier series terms very slowly decrease. As

Fig. 8. Amplitude of Fourier coefficients in the fluid-solid interface case.

a result, numerical estimation of G.M.I. approach can not provide reliable data, except for very high frequencies ($kr_s > 100$).

These three numerical examples illustrate various actual situations. In a global way, the computation is based on a compromise between the number of Fourier coefficients required to fit the reflection coefficient and the number of terms taken into account in the modal series. Assuming the reflection coefficient needs m_{max} Fourier coefficients to be well approximated, the modal series is convergent depending on whether $kr_s/2 \geq m_{max}$ or not. Most of time, the convergence can always be ensured if the frequency is high enough. In other words, the theory developed in this paper seems more adapted to higher frequencies for irregular coefficient reflection. Nevertheless, with smooth coefficient reflection function, our G.M.I. approach give reliable results even for a low frequency. More, in practice, physical models usually consider absorbing interfaces, and the influence of absorption phenomenon greatly improves the reliability of our modal approach.

In a computational point of view, the numerical integration of the plane wave spectra is far more time consuming than the summation of modal series, especially at high frequencies. Any way, the comparison between series and integral expression of the Green function constitutes a very simple way to estimate the numerical validity of the G.M.I. model. For a given frequency domain, the maximum error value can be easily computed whatever the interface may be.

4.3. *Evaluation of the scattering by cylinder-interface system*

Let us consider the scattering by a rigid circular cross section cylinder (radius denoted

by a) lying near the sedimentary media-fluid plane interface. Even for this rather simple problem, the scattered field has a complicated structure because of multiple interferences. The physical interpretation and the numerical estimation of the scattered field depends in a large way on the position on the observer. This is the reason why the following analysis of the scattered field is restricted to two "limited" regions, the first above the cylinder ($x = 0$, $y \leq h+a$), the other one between the cylinder and the interface ($x = 0$, $0 \leq y \leq h+a$), when the propagation direction of the incident wave is normal to the interface ($\alpha = 0$). In the first region, we perform a temporal analysis which consists in calculating the scattering of normal incident wideband wave (a short pulse represented by Dirac function in time domain). The purpose is to identify the different echoes which are responsible of the interferences. In the second region, we analyze the scattered field with respect to the altitude at a given frequency. In this way, we point out the interferential behavior of the scattered field.

It is noteworthy that the rigid cylinder problem is of interest for studying a more complex problem: the scattering by an elastic cylinder near a plane interface. As a matter of fact, when searching for the elastic cylinder resonances, without interface, the basic idea of the RST (Resonant Scattering Theory) is to remove the non resonant component usually called "background" [14,23,24]. For elastic cylinders, the background is defined from the scattering by the same cylinder (with the same external radius) assumed to be rigid [14,23,24]. Following the same idea, the rigid cylinder-interface system can be considered as the background corresponding to the elastic cylinder-interface system.

First of all, it is useful to recall the main properties of the scattering by rigid cylinders. With the use of the Sommerfeld-Watson transformation [25,26,27], one can show that the scattered field results from two physical contributions, i.e. the specularly reflected wave which is a geometric type wave, and the radiation of creeping waves also called "Franz waves" which are surface waves [25]. The creeping waves are generated at grazing angles and radiate tangentially from the surface when propagating around the cylinder. Their phase velocity is very close to the sound speed c_1 in the surrounding fluid, except at low frequency. Taking into account the frequency range investigated, the phase velocity of creeping waves will be approximated by c_1 for computations. It is also well known that the creeping waves are very attenuated and cannot turn for a long time around the cylinder. In practice, only the first Franz waves (usually denoted by $F_n^{(r)}$) can circumnavigate the cylinder farther than a half-turn.

4.3.1. *Temporal analysis*

The temporal analysis is carried out by using the Fourier transform applied to the incident pulse. As a result, the scattered pulse is the inverse Fourier transform of the scattered acoustic field given in Eq. (3.34). The so-obtained scattered pulse shows (see figure (9(a))) two important peaks that can be obviously associated to the specular reflection on the cylinder (A component) and the reflection by the interface (B component). Near after the peaks of the reflection by the interface two weak components (C and D) are observed in figure (9(b)).

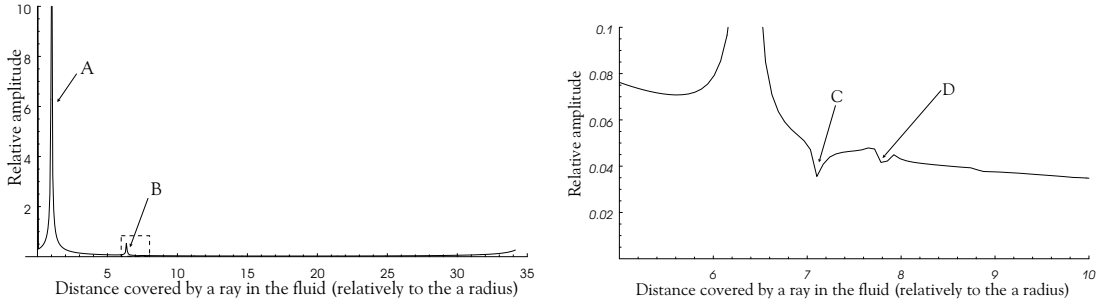

(a) General view. (b) Figure focused near after the B component.

Fig. 9. Temporal components caused by the incident pulse.

With the time of arrival of each peak and the sound speed c_1, the distances covered by these rays are computed. In figures (9), these distances are divided by the radius a to consider an dimensionless problem. The C component corresponds to the ray path depicted in figure (10(a)): the incident wave grazes the cylinder, is reflected by the interface, and the reflected wave generates the creeping waves which radiate toward the observer (M point). The ray path for the D component is quite similar to the previous one but with a cylinder-interface interaction: a double reflection by the plane interface and a reflection by the cylinder as shown in figure (10(b)).

The times of arrival of the four components (A,B,C and D) obtained from the G.M.I. computation are in agreement with those calculated with the geometrical theory of acoustic rays. In the case of a rigid cylinder-plane interface system, the scattered field results from a restricted number of Franz waves. Each peak observed in figures (9) can be easily related to a physical ray path. In more realistic configurations (elastic cylinder, non circular cross section cylinder,etc...), physical interpretations become far more ambiguous.

4.3.2. *Harmonic scattered field between the cylinder and the interface*

This analysis is performed by studying the acoustic field with respect to the altitude of the observer, denoted h_M, between the cylinder and the interface (the reduced frequency is $ka = 20$). Considering the Geometrical Theory of Diffraction (G.T.D.), the acoustic field observed in the interaction area can be approximated by the influence of three main rays, depicted in figure (11).

With the first acoustic ray, the creeping waves are generated at grazing incidence and radiate straightforwardly toward the observer (see figure 11(a)). With the second acoustic ray, the creeping waves insonifies the interface which reflects the waves toward the observer (see figure 11(b)). For the last acoustic ray, the waves reflected by the interface are once again reflected, by the cylinder, before propagating toward the observer (see figure 11(c)). The cylinder studied in this part is a rigid one, and so the creeping waves are restricted to the different modes of Franz waves. The numerical evaluation of each ray contribution is

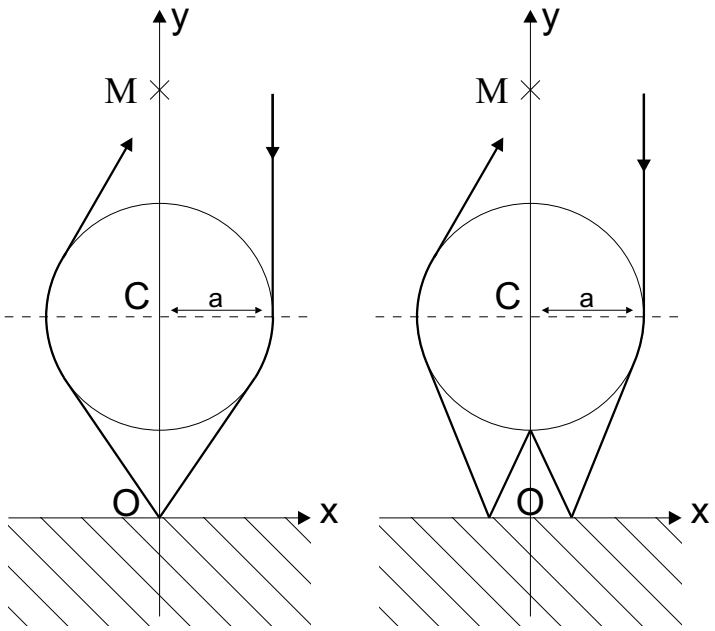

(a) C component. (b) D component.

Fig. 10. Ray path for the C and D components.

estimated using the Sommerfeld-Watson transform and taking into account the first three Franz modes. For the first ray path, the influence of a Franz mode is given by the well known expression [28]:

$$P1_{Fn} = -2\pi \frac{e^{-i\nu_{Fn}\pi/2}}{\sin \nu_{Fn}\pi} Res_{\nu_{Fn}} \left(T_{\nu\nu}\right) H^1_{\nu_{Fn}} \left(k \left(h - h_M\right)\right) \tag{4.53}$$

where ν_{Fn} is the pole for the Franz mode n, $T_{\nu\nu}$ is the complex function associated with the components of the $\mathbf{T}$ transition matrix and $Res_{\nu_{Fn}} \left(T_{\nu\nu}\right)$ is the residue of the $T_{\nu\nu}$ function and ν_{Fn} pole. The exact expression of the contribution for the two other ray paths can be quite easily deduced from Eq. (4.53) using geometrical tools (symmetry, ...). For example, the determination of the length of the third ray path leads to the resolution of an algebraic equation with degree four.

For our numerical example, the first three Franz wave poles are approximately, see [29]:

$$\nu_{F1} \simeq 21,07 + I1,95 \tag{4.54}$$

$$\nu_{F2} \simeq 23,45 + I6,14 \tag{4.55}$$

$$\nu_{F3} \simeq 25,10 + I9,16 \tag{4.56}$$

And the G.T.D. approximation of the acoustic field between the cylinder and the interface is the sum of each ray path for each Franz wave mode. Despite a non-negligible difference, the figure (12) show that the G.M.I. approach and the G.T.D. approximation are consistent.

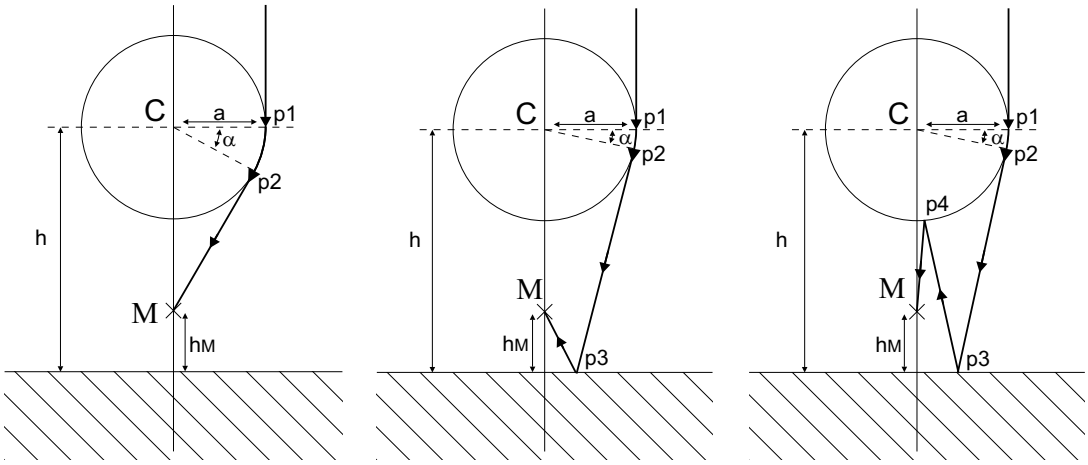

(a) Ray path 1. (b) Ray path 2. (c) Ray path 3.

Fig. 11. Main ray paths in the interaction area: h_M is the distance of the observer from the interface, α is the angle of the creeping wave path and (p_1, p_2, p_3, p_4) are the most characteristic points of the ray paths.

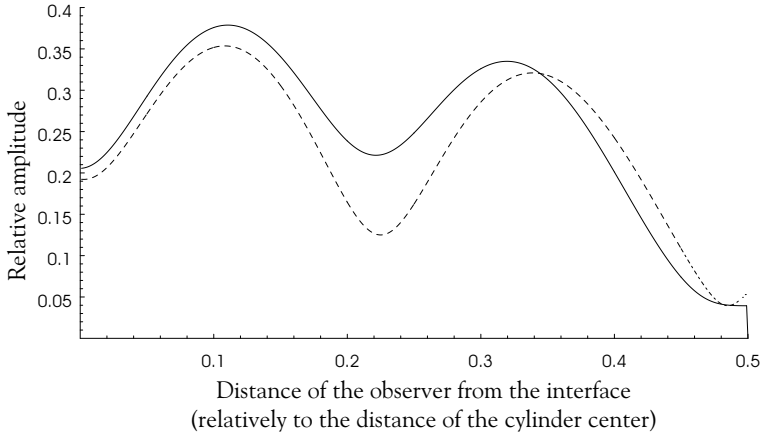

Fig. 12. Comparison between G.M.I. approach (plain line) and the G.T.D. approximation (dotted line).

Obviously, due to the great number of creeping waves, the G.T.D. approximation method becomes very difficult to apply when the cylinder is more complex. Thus, in common situations, the G.T.D. approach is inappropriate to estimate the acoustic field between the cylinder and the plane interface. On the other hand, the complexity of the G.M.I. algorithm in independent of the cylinder characteristics.

4.3.3. *Computational tractability*

To show the good computational tractability of the G.M.I. approach, the scattering by an elastic cylinder lying near a fluid-fluid interface is considered in this paragraph. The cylinder is a circular cross section hollow tube made of aluminum: density $\rho = 2790\ kg{\cdot}m^{-3}$, longitudinal velocity $c_L = 6557\ m \cdot s^{-1}$ and transversal velocity $c_T = 3128\ m \cdot s^{-1}$. The outer radius, denoted by a, is $a = 0.003572\ m$ and the inner radius, denoted by b, is defined as $b = 0.9\ a$.

The fluid-fluid interface corresponds to the first case studied in the numerical discussion section. The distance of the cylinder center from the interface is $h = 1.5\ a$, and the frequency is chosen so that the dimensionless product $ka = 20$. Figure (13) shows the acoustic field scattered by the cylinder-interface system. The ordinate and the abscissa of the observer are divided by the outer radius a to obtained dimensionless co-ordinates. The plane incident wave impinges the cylinder at a normal angle ($\alpha = 0$). Finally, to compute these 1000×1000 pixels, our algorithm only requires several minutes with a standard PC.

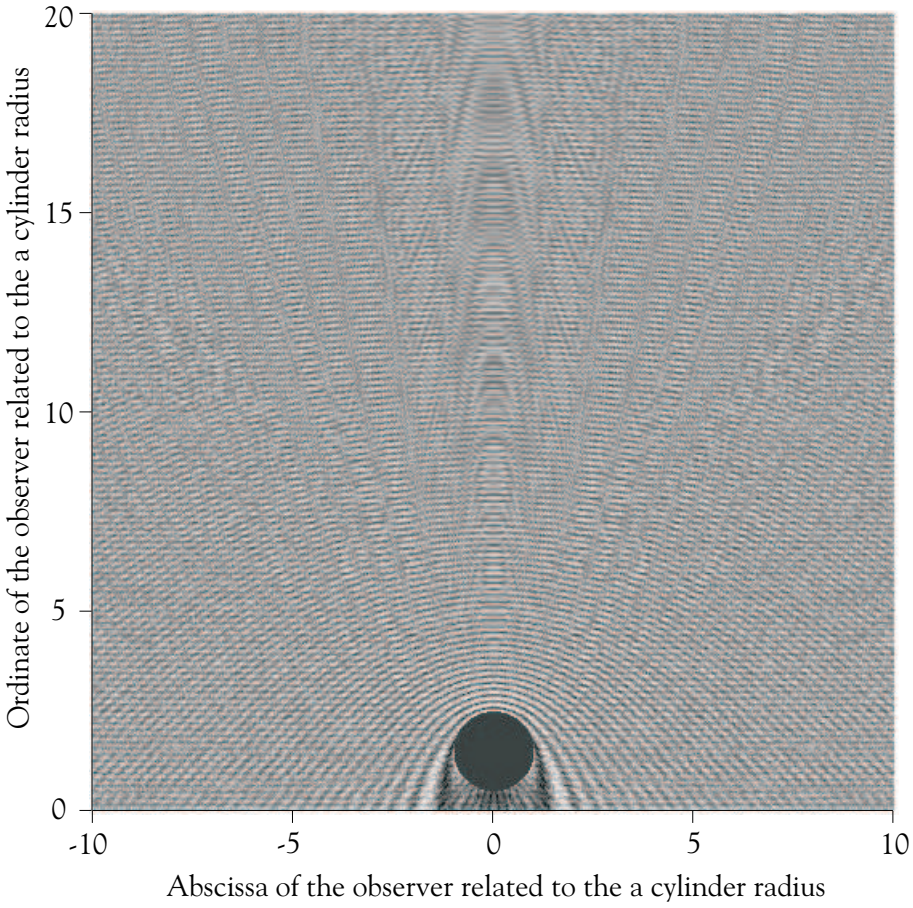

Fig. 13. Acoustic field scattered by an elastic tube-plane interface system.

5. Conclusion

An analytical theory has been developed in order to calculate the scattering by a cylinder lying near an elastic plane interface. The theory is based on the knowledge of both the **T** transition matrix describing the cylinder scattering and the $R(\theta)$ reflection coefficient of the plane interface. In this paper, our method is proved to be a generalization of the method of images commonly used for studying of the cylinder-(rigid or soft) interface system. More, our theoretical approach leads to an original expression for the two-dimensional Green function in the half-plane. Then, a great part of this article is devoted to the validity domain of the G.M.I. and the the comparison with the computations and the approximated curves obtained from the G.T.D. approximation. Physical interpretations for the cylinder-interface interactions were presented.

Thus, we show that the G.M.I. theory is particularly well adapted for analyzing the scattering at high frequencies, when the numerical methods limited to low frequencies do not work any longer. More, the use of the theory remains simple for studying more complex scatterer. For example, one can replace the circular cross section cylinder by an elliptical one with just changing the transition matrix **T**; for elliptical cylinders the transition matrix can be calculated from the T-matrix theory even for rather high frequencies [30]. It is also possible to take multilayered elastic plane interfaces into account. Due to the good computational tractability, the G.M.I. models constitutes an interesting theoretical and numerical tool to tackle identification and inverse problems solving. In consequence, the G.M.I. theory can be easily adapted to study elastic objects buried in a sediment with a plane surface [19], these works are in progress.

Acknowledgments

The authors would like to thank the reviewers for their helpful comments on the manuscript.

References

1. J.A. Fawcett, A plane-wave decomposition method for modelling scattering from objects and bathymetry in a waveguide, *J. Acoust. Soc. Am.*, **100**(1), pp.183–192, 1996.
2. M.F. Werby, C.G. Gaunaurd, Resonance in the backscattered echoes from elastic shells near an interface, In *Elastic Wave Propagation*, pages 393–398, Elsevier Science Publishers (North-Holland), mccarthy and hayes edition, 1989.
3. C.G. Gaunaurd, Distortions in the backscattering cross-section of a submerged elastic target produced by its proximity to the sea surface bottom, In *Computational Acoustics*, volume 2, pages 25–37, Elsevier Science Publishers (North-Holland), lee, cakmak and vichnevetsky edition, 1990.
4. G.C. Gaunaurd, H. Huang, Acoustic scattering by a spherical body near a plane boundary, *J. Acoust. Soc. Am.*, **96**(4), pp.2526–2536, 1994.
5. H. Huang, G.C. Gaunaurd, Acoustic point source scattering by a spherical elastic shell submerged beneath a free surface, *J. Acoust. Soc. Am.*, **99**(5), pp.2720–2726, 1996.
6. P.M. Morse, H. Feshbach, *Methods of Theoretical Physics*, McGraw-Hill, New-York, 1968.

7. D.E. Chimenti, A.H. Nayfeh, D.L. Butler, Leaky Rayleigh waves on a layered halfspace, *J. Acoust. Soc. Am.*, **53**(1), pp.170–176, 1982.
8. D.B. Bogy, S.M. Gracewski, Nonspecular reflection of bounded acoustic beams from the liquid-solid interface of two elastic layers on a halfspace under water, *Int.J.Solids.Structures*, **20**(8), pp.747–760, 1984.
9. A.H. Nayfeh, T.W. Taylor, Surface wave characteristics of fluid-loaded multilayered media, *J. Acoust. Soc. Am.*, **84**(6), pp.2187–2191, 1988.
10. L.M. Brekhovskikh, O.A. Godin, *Acoustics of layered media I. Plane and quasi-plane waves*, volume 5 of *Springer series on wave phenomena*, Springer-Verlag, Berlin, 1990.
11. J.J. Faran, Sound scattering by solid cylinders and spheres, *J. Acoust. Soc. Am.*, **23**, pp.405–418, 1951.
12. R.D. Doolittle, H. Überall, P. Uginčius, Sound scattering by elastic cylinders, *J. Acoust. Soc. Am.*, **43**, pp.1–14, 1968.
13. L. Flax, W.G. Neubauer, Acoustic reflection from layered elastic absorptive cylinders, *J. Acoust. Soc. Am.*, **61**, pp.307–312, 1977.
14. N.D. Veksler, *Resonance Acoustic Spectroscopy*, Springer-Verlag, 1993.
15. P.C. Waterman, New formulation of acoustic scattering, *J. Acoust. Soc. Am.*, **45**(6), pp.1417–1429, 1969.
16. P.C. Waterman, Symmetry, unitary, and geometry in electromagnetic scattering, *Phys. Rev.*, **3**(4), pp.825–839, 1971.
17. A. Sommerfeld, *Partial differential equations in physics*, Academic Press, New-York, 1949.
18. M. Abramowitz, I. Stegun, *Handbook of mathematical functions*, Dover Publications, New-York, 1965.
19. J.A. Fawcett, Acoustic scattering from cylindrical objects embedded between two half-spaces, *J. Acoust. Soc. Am.*, **100**(5), pp.3053–3060, 1996.
20. G.H. Hardy, *Divergent series*, Oxford University Press, New York, 1949.
21. W. Balser, *Formal Power Series and Linear Systems of Meromorphic Ordinary Differential Equations*, Springer-Verlag, New-York, 2000.
22. W.M. R. fiorito, H. Überall, Acoustic resonances and the determination of the material parameters of a viscous fluid layer, *J. Acoust. Soc. Am.*, **69**, pp.897–903, 1981.
23. L. Flax, L.R. Dragonette, H. Überall, Theory of elastic resonance excitation by sound scattering, *J. Acoust. Soc. Am.*, **63**, pp.723–731, 1978.
24. H. Überall, *Acoustic Resonance Scattering*, Überall, Gordon and Breach Science Publishers, New-York, 1992.
25. G.V. Frisk, H. Überall, Creeping waves and lateral waves in acoustic scattering by large elastic cylinders, *J. Acoust. Soc. Am.*, **59**, pp.46–54, 1976.
26. P.L. Marston, GTD for backscattering from elastic spheres and cylinders in water and the coupling of surface elastic waves with the acoustic field, *J. Acoust. Soc. Am.*, **83**(1), pp.25–37, 1988.
27. J.M. Conoir, J.L. Izbicki, P. Rembert, *Acoustic Interaction With Submerged Elastic Structures*, chapter Scatering by cylindrical objects at oblique incidence, pages 81–128, Stability Vibration and Control of Systems, Guran, Ripoche and Ziegler, World Publishers, 1996.
28. N. Gespa, *La diffusion acoustique par des cibles élastiques de forme géométrique simple. Théories et expériences*, Imprimerie du CEDOCAR, Paris, 1987.
29. B. Clotteau, J.M. Conoir, J.L. Rousselot, A. Derem, Ondes de Franz et onde de Stoneley généralisées pour un cylindre élastique immergé, *J. Acoustique*, **3**(3), pp.213–242, 1990.
30. V. Varadan, Scattering matrix for elastic waves. II., *J. Acoust. Soc. Am.*, **63**(4), pp.1014–1024, 1978.